Available online at www.eccomasproceedia.org
Eccomas Proceedia COMPDYN (2023) 2369-2379

ECCOMAS
Proceedia

COMPDYN 2023
9th ECCOMAS Thematic Conference on
Computational Methods in Structural Dynamics and Earthquake Engineering
M. Papadrakakis, M. Fragiadakis (eds.)
Athens, Greece, 12-14 June 2023

UNCERTAINTY QUANTIFICATION IN THE CONSTITUTIVE BEHAVIOR OF HDRBs

José A. Gallardo[1,2], Juan C. de la Llera[1,2], and Katrin Beyer[3]

[1]Department of Structural and Geotechnical Engineering, Pontificia Universidad Catolica de Chile, Santiago, Chile
jogallardo@uc.cl, jcllera@ing.puc.cl

[2]Research Center for Integrated Disaster Risk Management (CIGIDEN), Santiago, Chile
jogallardo@uc.cl, jcllera@ing.puc.cl

[3]Earthquake Engineering and Structural Dynamics Laboratory (EESD)
School of Architecture, Civil and Environmental Engineering, École Polytechnique Fédérale de Lausanne (EPFL), Lausanne, Switzerland
katrin.beyer@epfl.ch

Abstract. *High Damping Rubber Bearings (HDRBs) are widely used in seismic isolation of structures, and their force-deformation constitutive behavior controls the lateral structural response during an earthquake. However, given the many components and steps involved in the preparation of the rubber compound and the manufacturing process itself, the HDRB force-deformation behavior presents significant variability with respect to nominal design values. Consequently, this paper proposes a framework for parametric probabilistic modeling of the uncertain behavior of these devices. For the validation of this framework, a recently proposed force-deformation phenomenologically based numerical model is considered. Calibration of the HDRB model is based on experimental results of 125 devices and uses the Covariance Matrix Adaptative Evolution Strategy (CMA-ES) algorithm to fit the model parameters. Since the structural response is controlled by the isolator behavior, this parametric probabilistic model provides an efficient tool to propagate uncertainty from the isolation devices to the final dynamic response of the structure. This framework can also be used to evaluate the validity of the approximate code methodology of the upper and lower bound isolator property design limits, which are applied for all isolators simultaneously.*

Keywords: Uncertainty quantification; Parametric probabilistic modeling; High damping rubber bearings; Seismic isolation.

ISSN:2623-3347
Peer-review under responsibility of the organizing committee of COMPDYN 2023.
doi: 10.7712/120123.10566.21057

1 INTRODUCTION

The force-deformation constitutive relationship of seismic isolation devices dominates the dynamic response of isolated structures. Therefore, an accurate characterization of isolator behavior is critical in evaluating seismic performance. High Damping Rubber Bearings (HDRBs) are probably one of the most used isolation devices in practice; however, modeling their behavior still present challenges due to their high non-linearity. The characterization of HDRB behavior also includes the uncertainty in the force-deformation response of devices with equal nominal properties, as this uncertainty affects the response of structures significantly. The source of this uncertainty arises from the intrinsic variability of the rheological properties of the rubber compound, which increases with the manufacturing process since it is extremely sensitive to temperature, pressure, and rubber curing time [1]. Additionally, the misalignment of the steel shims within the device also influences the lateral and vertical behavior [2].

Design standards account for this uncertainty in HDRBs by means of two approaches: (i) using modification factors to establish lower and upper bounds [3]; or (ii) defining the most unfavorable set of parameters [4, 5]. It is worth noting that the former includes effects such as scragging within the uncertainty factor, while the latter relies on professional judgment to define parameter values. In the literature, uncertainty has been commonly quantified in terms of dissipated energy capacity and effective stiffness [6, 7], which is a reasonable assumption since these two parameters are the most used in the design process.

During last two decades, several numerical models have been proposed to simulate the behavior of HDRBs, most of them are phenomenological models which try to include several phenomena, such as strain-rate dependency [8, 9], stress softening [10, 11], and load direction dependency [12, 13]. Some of these characteristics of the HDRB behavior, such as the stiffening observed at large deformations, has significant influence in the dynamic response of seismically isolated structures [14]. These models usually require a large number of parameters to define the force-deformation response. The use of these models in quantifying uncertainty propagation from HDRB properties to the dynamic response of seismically isolated structures is not found in the current literature. This is in part because of the limited availability of experimental data, which makes difficult to generate parametric probabilistic models. This research work proposes a useful tool to encourage the use of sophisticated phenomenological models in uncertainty quantification of seismically isolated structures that use HDRBs. A data augmentation technique is presented to overcome data limitations, which is also validated. This data augmentation technique can be classified as oversampling, and takes advantage of the non uniqueness of optimal parameters for phenomenological based numerical models.

The aim of this paper is twofold: (i) to present a data augmentation technique for phenomenological based numerical models; and (ii) to propose a framework for parametric probabilistic modeling of HDRBs to consider random uncertainty. In Section 2 the manuscript describes the case-study and the experimental data; Section 3 outlines the generation of the parametric probabilistic model; Section 4 shows the results and comparisons between the artificial devices generated using the proposed model and the experimental database; and Section 5 finally presents conclusions of this study.

2 EXPERIMENTAL DATA AND MODELING ASSUMPTIONS

The nominal device used for this research is an annular-shaped HDRB, which outer (D_o) and inner diameter (D_i) are 70 and 10 cm, respectively. The bearing consists of 34 rubber layers 6 mm thick, 33 steel shims 3 mm thick, and upper and bottom steel plates 30 mm thick. The

total height of the device is 363 mm, while the total height of elastomeric material (H_r) is 204 mm. The shape factor (S), computed as the ratio of the loaded and the free to deform area, is 25. The nominal shear modulus (G) of the elastomeric material is 5 kgf/cm^2. The considered device was used in the seismic isolation system of an actual hospital in Santiago, Chile. Figure 1a sketches the HDRB used in this work.

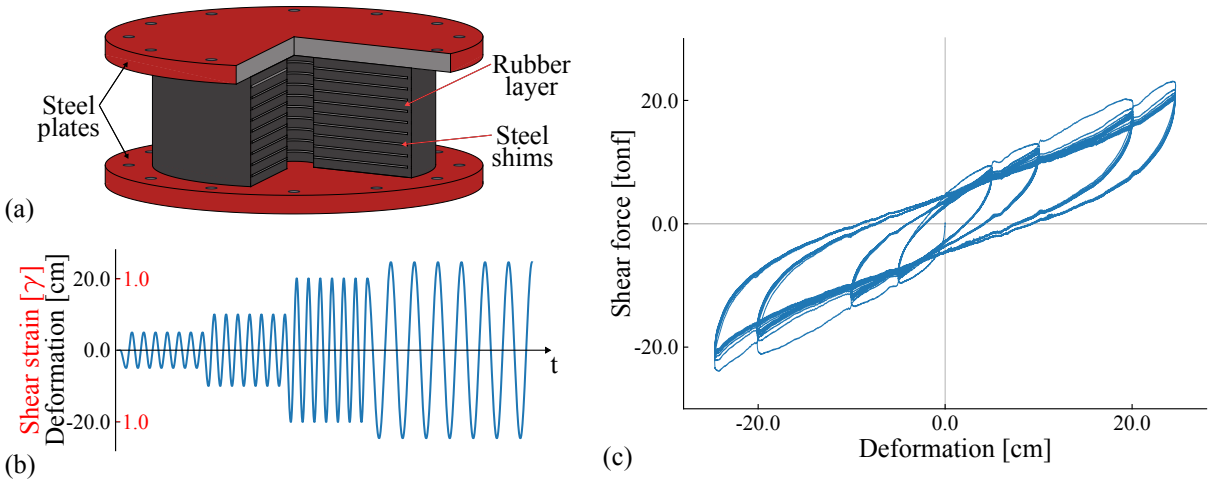

Figure 1: HDRB: a) simplified sketch of the device; b) deformation history of tests; and c) force-deformation constitutive behavior.

2.1 Experimental database

The experimental data used in this research includes the results of all devices ready for installation as part of the isolation system after quality control testing, which accounts for 125 HDRBs. The load pattern of the experimental tests was applied in two phases: phase 1 considered a compressive load of 345 tonf, resulting in a compressive stress of 91.51 kgf/cm^2; and phase 2 considered a cyclic lateral deformation history including four different strain levels (25, 50, 100, and 123 %) with seven full cycles at each strain level at a fixed frequency of about 0.08Hz. Figures 1b and 1c show the imposed deformation history and shear force-deformation experimental response of a device randomly selected from the database, respectively.

2.2 Numerical model for HDRBs

A recently proposed force-deformation model [13] is used in this research for simulating the shear response of the devices. The numerical shear model includes phenomena such as stress softening with unilateral effect (anisotropy induced by degradation), temporary hardening, and stiffening at large deformations. The mathematical formulation is based on a decomposition of the force-deformation constitutive relationship into a hyperelastic and a dissipative component working in parallel thus, $F = F_h + F_d$, where F, F_h, and F_d, are the total shear force, the shear force of the hyperelastic, and the shear force of the dissipative component, respectively. This model fits qualitatively and quantitatively well the experimental results of HDRBs; a summary of the mathematical formulation of the shear model is presented in Table 1, and the complete formulation can be found elsewhere [13].

The shear model requires the calibration of 17 parameters (Table 1): three for the hyperelastic component (a_{10}, a_{20}, a_{30}), four for the dissipative component (κ, f_y, β, η), eight for the stress

Table 1: Constitutive equations of the shear model [13].

Hyperelastic component	Dissipative component
$F_h = K_{s1}K_m a_{10}\gamma - K_{s2}a_{20}\gamma^3 + K_{s3}a_{30}\gamma^5$	$F_d = f_y z$
Scragging	*Evolution law*
$K_{s1} = \exp(-C_1\gamma_s^{p_1})$	$\dot{z} = \frac{k}{f_y}\dot{\gamma}\left[1 - \lvert z\rvert^{\eta} R\right]$
$K_{s2} = K_{s1}\exp(-C_2\gamma_s^{p_2})$	$R = \beta\text{sign}(\dot{\gamma}z) + \alpha - \Phi\text{sign}(\dot{\gamma})\left(\text{sign}(z) + \text{sign}(\dot{\gamma})\right)$
$K_{s3} = K_{s1}\exp(-C_3\gamma_s^{p_3})$	*Temporary hardening*
$\gamma_s^{\pm} = \min\left(\gamma_{hp}^{\pm}, \gamma_{s(trial)}^{\pm}\right)$	$\Phi = \Phi_{max}\left[1 - \exp\left(-P_\Phi\left\lvert\frac{\gamma_{pl}}{\gamma_y}\right\rvert\right)\right]$
$\dot{\gamma}_{s(trial)}^{\pm} = \begin{cases} \frac{\lvert\dot{\gamma}\rvert}{2}, \text{ for loading} \\ 4\lvert\dot{\gamma}\rvert, \text{ for unloading} \end{cases}$	
Mullins effect	
$K_m = \exp(-C_m\gamma_m^{p_m})$	
$\dot{\gamma}_m^{\pm} = \begin{cases} 0, \text{ for loading} \\ \lvert\dot{\gamma}\rvert, \text{ for unloading} \end{cases}$	

softening (C_1, p_1, C_2, p_2, C_3, p_3, C_m, p_m), and two for defining the temporary hardening ($\Phi_{\max}$, P_Φ).

The coupling between axial and shear response was considered using the two spring model [15]. However, the two parameters of this model (stiffness of the two springs) were considered constant and calculated according to the traditional theoretical formulation [16], they do not participate in the development of the parametric probabilistic model.

2.3 Parameter calibration

The 17 parameter values were estimated to match the data obtained from experimental results of HDRBs. This parameter calibration was performed using the Covariance Matrix Adaptation Evolution Strategy (CMA-ES) [17]. This is a stochastic optimization algorithm that uses previous iteration results to determine the evolution path of descendants. For this process, we considered 100 steps with 20 descendants in each step. The optimization objective was to minimize the mean squared error (Ψ) between the experimentally measured and the model simulated forces for each sampled deformation, i.e,

$$\text{Minimize}\left\{\Psi = \frac{1}{n}\sum_{i=1}^{n}\left(f_i^t - f_i^m\right)^2\right\} \tag{1}$$

where n is the number of sampled deformations, and f_i^t and f_i^m are the experimental and model forces at the i-th sampled deformation, respectively.

Since the model parameters for simulating the shear response of HDRBs are related in a highly non-linear way, the optimal set of values for matching the experimental response of each device is not unique [18]. The set of parameters resulting from the optimization depends on the initialization parameter of the algorithm that generates the descendants within the optimization algorithm. This is because the descendants in the first step of the optimization process define a path for the parameters (gradient). Thus, different descendants give different paths, and as a consequence, the optimization algorithm converges to a different set of values.

Table 2 shows the resulting numerical values of two different optimization processes and

Table 2: Parameter values for two different optimization processes.

Case	Ψ	a_{10}	a_{20}	a_{30}	C_1	p_1	C_2	p_2	C_3	p_3
Set 1	0.2297	74.53	89.25	266.67	1.19	0.27	35.90	0.29	3.08	0.32
Set 2	0.2270	56.05	55.79	185.90	0.85	0.40	34.81	0.48	3.07	0.23

Case	C_m	p_m	κ	f_y	β	η	$\Phi_{\max}$	P_Φ
Set 1	0.078	0.34	157.42	2.05	0.90	0.32	0.20	0.0033
Set 2	0.097	0.35	173.87	1.80	0.90	0.30	0.15	0.0049

the value of Ψ in each case. Although the parameter values show significant differences, the Ψ values are very similar. Figure 2 presents the simulation results considering both sets of parameter values presented in Table 2, and the differences between both curves are almost negligible. We are currently thinking of ways of constraining better this optimization process, so the solution also maintains the desirable properties of models used typically in isolation design.

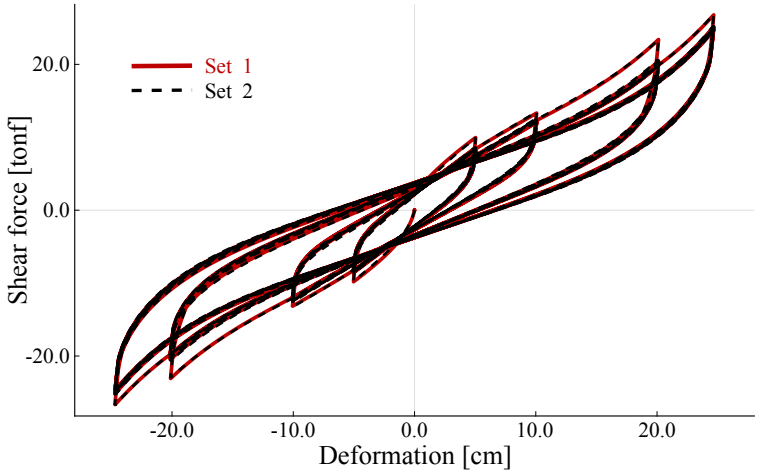

Figure 2: Simulated response considering two sets of parameter values: a) Set 1, and b) Set 2 (Table 2).

3 PARAMETRIC PROBABILISTIC MODELING

A parametric probabilistic model considers the definition of the Probability Density Functions (PDFs) for each unknown parameter, the estimation of the PDFs parameters, and the estimation of the correlations between the unknown parameters. All this depends on the data, which sometimes is very limited in practice, affecting the quality of the probabilistic model due to undesired biases. In fields such as image processing, a common practice to overcome this limitation is to augment the database by manipulating the existing samples [20]. Consequently, this section presents a data augmentation technique for phenomenological-based numerical models.

3.1 Data augmentation

The data augmentation technique takes advantage of the non-uniqueness of the optimal set of parameter values for matching an experimental test response [18]. With the aim to validate this technique, we separate from the total sample a subset of 13 devices, i.e., 10% of the complete

dataset.

We start the process with the parameter calibration described in the previous section for the complete database of experimental test results. These results will be referred hereafter as the control data (CD). Then, the model calibration process is repeated ten times to match only the experimental results for the subset of 13 devices. Each process uses a different set of initialization parameter values for the optimization algorithm; the results of each calibration process will be denoted as a batch. Each batch includes 13 sets of parameter values for the shear model of the 13 HDRBs. Since we repeat the process ten times, we get ten batches. Given the non-uniqueness of the optimal parameters, each optimization process converges to different sets of parameters for each device, and hence, the corresponding sets of parameters for each device in two different batches are different.

3.2 Probabilistic models

The probabilistic models are generated considering the data corresponding to the 13 HDRBs of the subset, and the effectiveness of the data augmentation technique is verified selecting three data sizes (number of batches) and comparing that with the CD. The first model (Model 1) considers the data of just one calibration process (DM1), batch 1; the second model (Model 2) considers the data of three calibration processes (DM2), batches 1, 2 and 3; and the third model (Model 3) considers data of all ten calibration processes (DM3), batches 1 through 10. Thus, DM1 has an equal number of samples as HDRBs in the subset (13); DM2 has a number of samples equal to three times the number of HDRBs in the subset (39); and DM3 has a number of samples equal to ten times the number of HDRBs in the subset (130).

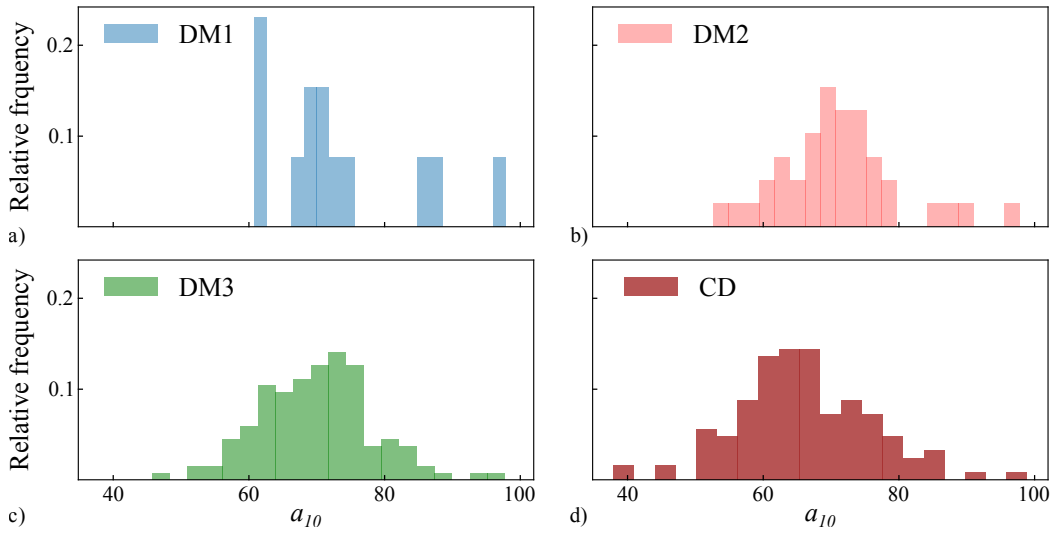

Figure 3: Relative frequency histograms for variable a_1: a) DM1, b) DM2, c) DM3, and d) CD.

Figure 3 shows an example of the relative frequency histograms of one model parameter, a_{10}. It is apparent that the DM1 dataset is not enough for capturing the distribution of the variable and presents a large bias. DM2 represents better the distribution of the variable, and the representation improves with DM3. Indeed, the histogram of DM3 is quite similar to that of CD. Because all parameter values need to be positive and considering as reference the DM3 dataset histograms, we chose log-normal distributions for essentially all model parameters, except for parameters β and η, which show low variability for the available data and, hence, are consid-

ered constant hereafter, with values equal to 0.90 and 0.30, respectively (Table 1, dissipative component).

Table 3 shows the mean values μ, and the coefficients of variation V, for all parameters considering the DM1, DM2, DM3, and CD datasets. Although there is no clear trend for all cases, it seems that increasing the number of samples with the data augmentation technique improves the estimation of the mean values, using CD as the target. Examples of this are the parameters a_{10} and κ. As it should, the values of the coefficient of variation V for the CD tend to be larger than the corresponding values for the other three cases.

Table 3: Mean values μ, and the coefficients of variation V, for parameters of the shear model considering DM1, DM2, DM3, and CD.

	DM1		DM2		DM3		CD	
Parameter	μ	V	μ	V	μ	V	μ	V
a_{10}	73.191	0.1437	70.800	0.1252	69.964	0.1193	65.985	0.1515
a_{20}	77.916	0.1792	76.641	0.1802	75.779	0.1801	78.369	0.2150
a_{30}	238.41	0.1640	232.60	0.1580	229.71	0.1787	229.77	0.2010
C_1	1.1171	0.1034	1.0907	0.0958	1.0809	0.1016	1.0779	0.1467
p_1	0.3121	0.1998	0.3219	0.1660	0.3251	0.1448	0.3036	0.1700
C_2	26.328	0.1582	28.223	0.1520	27.480	0.1779	28.191	0.1894
p_2	0.3419	0.1320	0.3602	0.2130	0.3708	0.1967	0.3421	0.2163
C_3	3.3680	0.0691	3.3793	0.0675	3.3703	0.0763	3.4909	0.0896
p_3	0.2511	0.2073	0.2434	0.1930	0.2461	0.1859	0.2378	0.1928
C_m	0.0913	0.2091	0.0920	0.1987	0.0901	0.1982	0.0873	0.2313
p_m	0.3145	0.1768	0.3082	0.1682	0.3134	0.1548	0.3056	0.1696
κ	150.25	0.1843	141.89	0.1569	141.86	0.1340	131.87	0.1453
f_y	2.9149	0.0792	2.9423	0.0874	2.9425	0.1004	2.7026	0.1438
$\Phi_{\max}$	0.1756	0.0773	0.1780	0.1032	0.1785	0.1310	0.1826	0.1696
P_Φ	0.0045	0.1465	0.0047	0.1713	0.0047	0.1837	0.0048	0.1752

Since log-normal distributions describe the values of the parameters, the mean of the natural logarithm of an arbitrary parameter λ_X, and its standard deviation ϵ_X, can be determined from the values presented in Table 3 using the following expressions [19],

$$\epsilon_X^2 = \ln\left(1 + V_X^2\right) \tag{2}$$

$$\lambda_X = \ln\left(\mu_X\right) - \frac{1}{2}\epsilon_X^2 \tag{3}$$

where X denotes the selected parameter.

Figure 4 shows the Pearson correlation matrices of the natural logarithm of the $17 - 2 = 15$ (fixed) parameters for DM1, DM2, DM3, and CD. For this table, the natural logarithm of all parameter values was computed, and then, the correlation matrix was determined. For the DM1 dataset, there are several parameters with large values of cross correlation. The number of parameters with large cross correlation values decreases for DM2 and DM3. In the comparison with the CD, it is apparent that the correlation matrix for DM3 is the closest, demonstrating that

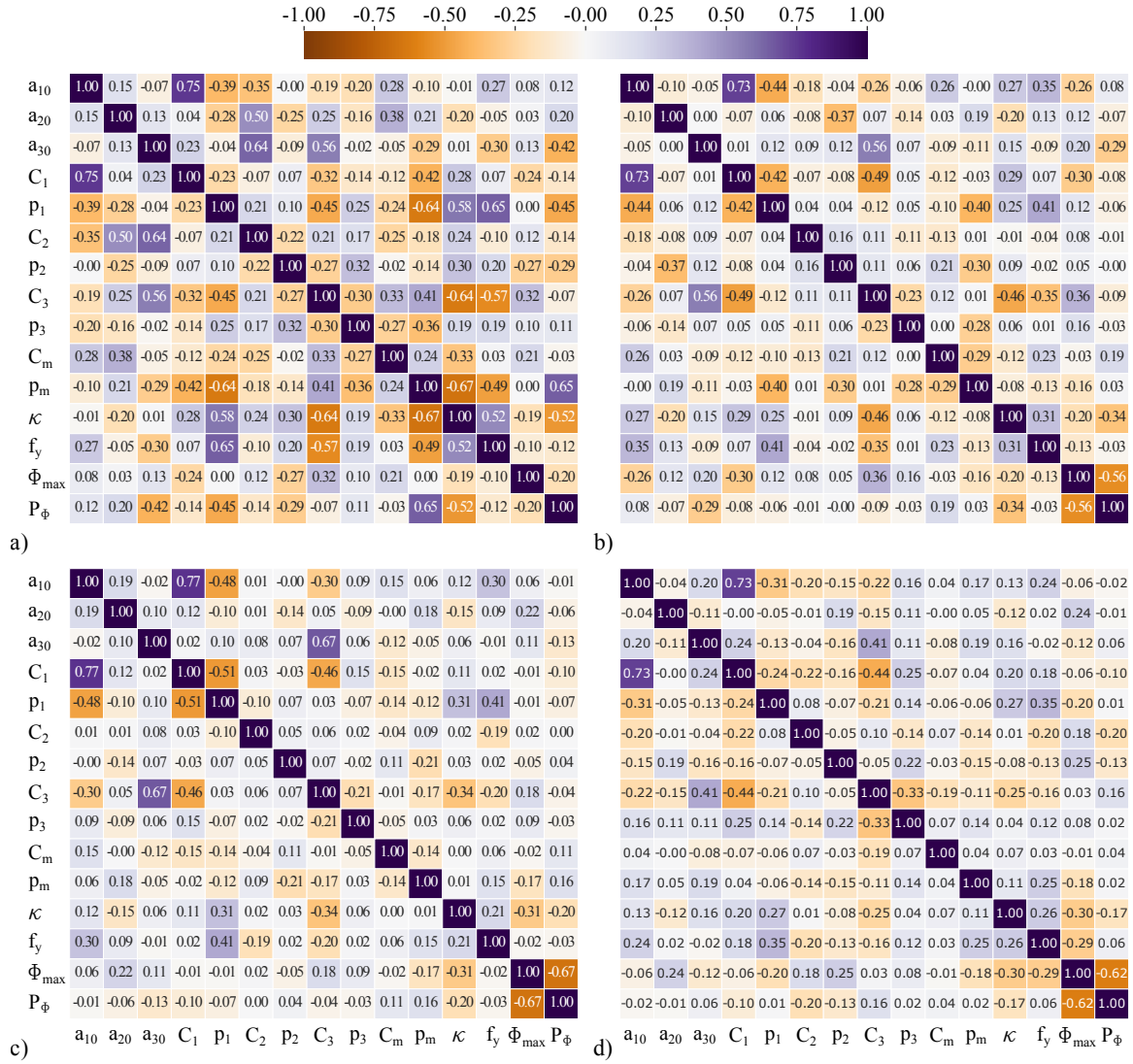

Figure 4: Pearson correlation matrices (C_r) for a) DM1, b) DM2, c) DM3, and d) CD.

the augmentation data technique avoids spurious large correlation values as result of the small number of samples.

4 RESULTS

The data of Table 3 and Figure 4 was used in the generation of the sets of parameters of artificial (synthetic) devices. A total of 125 sets of parameters was simulated for each case (DM1, DM2, and DM3), which is equal to the number of HDRBs of the complete dataset. This simulation was performed using the procedure presented in [19]. For the generation of the cross correlated parameters, the calculation of the eigenvalues of the covariance matrix $\boldsymbol{COV}$ is required, which can be computed as

$$\boldsymbol{COV}_{(i,j)} = \boldsymbol{\epsilon}_i \boldsymbol{Cr}_{(i,j)} \boldsymbol{\epsilon}_j \tag{4}$$

where $\boldsymbol{\epsilon}_i$ is the standard deviation of the i-th parameter computed using Eq. (2), and $\boldsymbol{C}_r$ is the correlation matrix (Figure 4).

Using the information of DM1, the resulting eigenvalues of the covariance matrix are complex numbers, and then, it is not possible to generate its corresponding sets of parameters. The

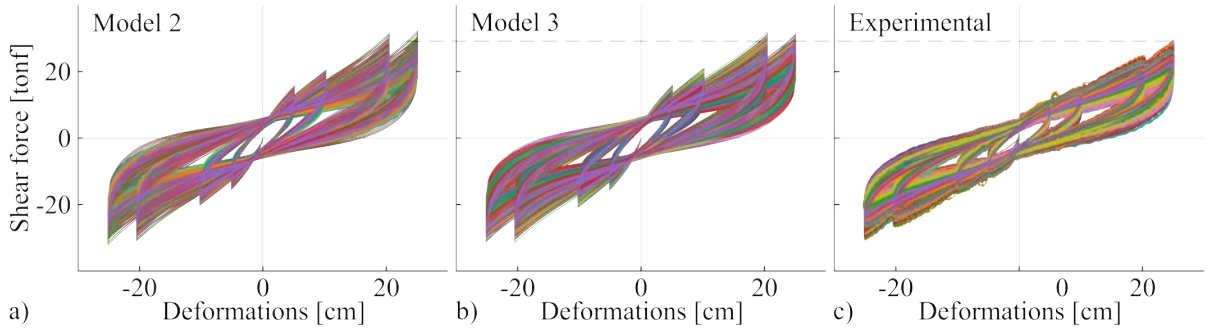

Figure 5: Comparison of artificial devices generated with a) Model 2, and b) Model 3, and c) experimental results.

response of the simulated devices using DM2 and DM3, and the experimental results of the 125 HDRBs, are plotted in Figure 5. Both cases show reasonably good agreement with the experimental results of the force-deformation constitutive relationships. However, numerically, the artificial devices generated considering DM3 present parameters more consistent with the experimental results of large databases in terms of mean values and correlations (Table 3 and Figure 4, respectively).

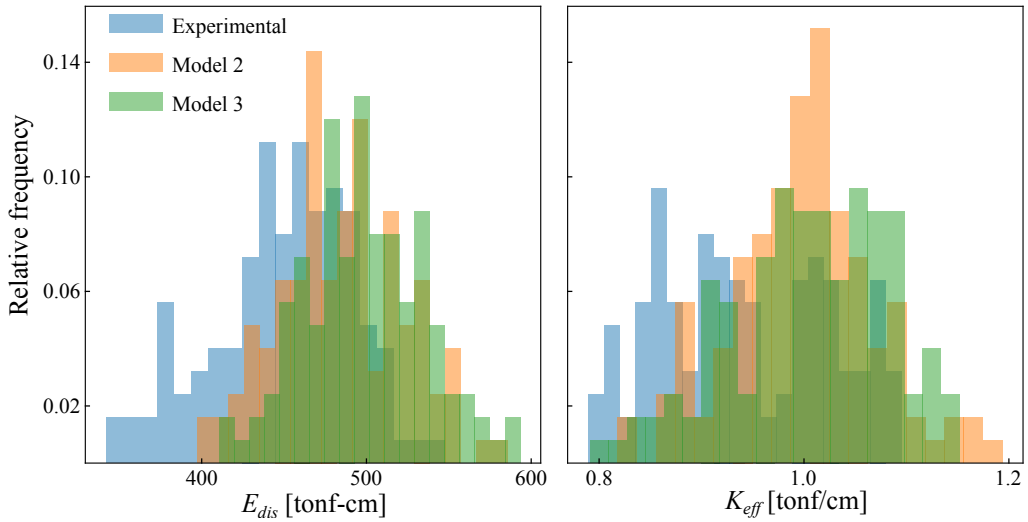

Figure 6: Relative frequency histograms of dissipated energy E_{dis} and effective stiffness K_{eff} computed at the third cycle of the larger shear strain for the two models and the experimental data.

Figure 6 shows the relative frequency histograms of dissipated energy (E_{dis}) and effective stiffness (K_{eff}) during the third cycle of the larger shear strain amplitude ($\gamma = 123\%$). This cycle was plotted because it represents the stable behavior of the device (after scragging). Both numerical models tend to slightly overestimate the dissipated energy and effective stiffness of the experimental test results, which is a consequence of bias in the selected subset used to calibrate the parametric probabilistic model, but there are negligible differences between both models.

5 SUMMARY AND CONCLUSIONS

This manuscript presents a framework for parametric probabilistic modeling of a phenomenological numerical model recently proposed for simulating the shear response of HDRBs. A data

augmentation technique is proposed, which takes advantage of the non-uniqueness of the optimal parameters for this type of numerical models. The data augmentation technique can be classified as oversampling, and is a good tool to overcome data limitation and reduce bias in small size databases. The technique reduces spurious large correlation between model parameters as a consequence of the limited number of experimental data. The parametric probabilistic model simulates well the uncertainty of shear behavior of HDRBs with the same nominal properties. Although the probabilistic models were developed considering only the experimental responses of 13 devices, the responses of the artificial devices generated with Model 2 (DM2) and Model 3 (DM3) fit reasonably well with the complete dataset of 125 HDRBs. This probabilistic model provides an efficient tool to characterize and propagate uncertainty from the HDRBs to the final dynamic response of seismically isolated structures. This framework can also be used to evaluate the validity of the approximate code methodology of the upper and lower bound isolator property design limits [3]. Moreover, the framework is useful for studying other topics such as accidental torsion in seismically isolated structures.

ACKNOWLEDGMENTS

This research has been sponsored by ANID/doctorate scholarship/ 21201370; Research Center for Integrated Disaster Risk Management (CIGIDEN), ANID/ FONDAP/ 1522A0005; and FONDECYT project, Multiscale earthquake risk mitigation of healthcare networks using seismic isolation, ANID/ FONDECYT/ 1220292.

REFERENCES

[1] A. Bhowmick , M. Hall & H. Benarey (Eds.), Rubber products manufacturing technology, *Marcel Dekker*, 1994.

[2] S. Ahmadi Soleimani, D. Konstantinidis, & G. Balomenos, Effect of manufacturing imperfections on the service-level performance of elastomeric bridge bearings, *Journal of Structural Engineering*, 148(7), 04022088, 2022.

[3] ASCE/SEI 7, Minimum design loads and associated criteria for buildings and other structures. *American Society of Civil Engineers*, 2022.

[4] British Standards Institution, Eurocode 8: Design of structures for earthquake resistance-part 1: general rules, seismic actions and rules for buildings. *Brussels: European Committee for Standardization*, 2005.

[5] INN, NCh2745 - Analysis and design of buildings with seismic isolation (in Spanish). *Instituto Nacional de Normalización*, 2013.

[6] RINTC Workgroup, Results of the 2015-2017 Implicit seismic risk of code-conforming structures in Italy (RINTC) project. *Rete dei Laboratori Universitari di Ingegneria Sismica (ReLUIS)*, 2018.

[7] S. Miranda, J. de la Llera, & E. Miranda, Uncertainty on measurement of elastomeric isolators effective properties, *Measurement*, 180, 109511, 2021.

[8] R. Jankowski, Nonlinear rate dependent model of high damping rubber bearing. *Bulletin of Earthquake Engineering*, 1(3): 397–403, 2003.

[9] A. Bhuiyan, Y. Okui, H. Mitamura, & T. Imai, A rheology model of high damping rubber bearings for seismic analysis: Identification of nonlinear viscosity. *International Journal of Solids and Structures*, 46(7-8): 1778–1792, 2009.

[10] J. Hwang, J. Wu, T. Pan, & G. Yang, A mathematical hysteretic model for elastomeric isolation bearings. *Earthquake Engineering & Structural Dynamics*, 31(4): 771–789, 2002.

[11] D. Grant, G. Fenves, & A. Whittaker, Bidirectional modelling of high-damping rubber bearings. *Journal of Earthquake Engineering*, 8(spec01): 161–185, 2004.

[12] E. Tubaldi, L. Ragni, A. Dall'Asta, H. Ahmadi, & A. Muhr, Stress softening behaviour of HDNR bearings: modelling and influence on the seismic response of isolated structures. *Earthquake Engineering & Structural Dynamics*, 46(12): 2033–2054, 2017.

[13] J. Gallardo, J.C. de la Llera, J. Restrepo & M. Chen, A numerical model for non-linear shear behavior of high damping rubber bearings. *Under Review*, 2023.

[14] C. Alhan, H. Gazi, & H. Kurtuluş, Significance of stiffening of high damping rubber bearings on the response of base-isolated buildings under near-fault earthquakes. *Mechanical Systems and Signal Processing*, 79, 297-313, 2016.

[15] K. Ryan, J. Kelly, & A. Chopra, Nonlinear model for lead–rubber bearings including axial-load effects. *Journal of Engineering Mechanics*, 131(12), 1270-1278, 2005.

[16] J. Kelly, & D. Konstantinidis, Mechanics of rubber bearings for seismic and vibration isolation. *John Wiley & Sons*, 2011.

[17] N. Hansen & A. Ostermeier, Completely derandomized self-adaptation in evolution strategies. *Evolutionary Computation*, 9 (2) 159–195, 2001.

[18] R. Ogden,, G. Saccomandi, I. Sgura, Fitting hyperelastic models to experimental data. *Computational Mechanics*, 34(6), 484-502, 2004.

[19] A. Nowak, & K. Collins, Reliability of structures. *CRC press*, 2012.

[20] C. Shorten, & T. Khoshgoftaar, A survey on image data augmentation for deep learning. *Journal of Big Data*, 6(1), 1-48, 2019.